

Stable Quantum Vortices in Lee-Huang-Yang Dipolar Superfluids

S. Sabari^(a), R. Radha^(b), Lauro Tomio^(a) and B. A. Malomed^(c,d)

^(a)*Instituto de Física Teórica, Universidade Estadual Paulista, 01140-070 São Paulo, SP, Brazil.*

^(b)*Centre for Nonlinear Science(CeNsc), Department of Physics, Government College for Women(A), Kumbakonam 612001, India.*

^(c)*Department of Physical Electronics, School of Electrical Engineering, Faculty of Engineering, and Center for Light-Matter Interaction, Tel Aviv University, P.O.B. 39040, Ramat Aviv, Tel Aviv, Israel.*

^(d)*Instituto de Alta Investigación, Universidad de Tarapacá, Casilla 7D, Arica, Chile.*

(Dated: January 28, 2026)

The nucleation and dynamics of vortices in the quasi-two-dimensional rotating dipolar Bose-Einstein condensate are explored by taking into account the Lee-Huang-Yang (LHY) correction to the mean-field (MF) theory. Assuming approximate cancellation of the MF interactions, we focus on the formation of a pure LHY superfluid. The effect of rotational frequency Ω is investigated numerically by determining the corresponding number of stable vortices in the superfluid, together with the respective energy per particle E and chemical potential μ . The LHY superfluid provides a deep minimum of E and μ , indicating that it is a remarkably robust state of quantum matter. By fixing the LHY interaction strength, an exact single-vortex critical frequency is found, along with the respective chemical potential. A notable feature, observed when creating the LHY superfluid with fewer than five vortices, which is understood as being due to the superfluid's nonlinearity and trapping aspect ratio, is the large frequency ranges admitting the production of two and four vortices, as compared to the small frequency ranges to obtain one and three vortices.

I. INTRODUCTION

The experimental observation of dipolar Bose-Einstein condensates (BECs) in ultracold gases of ^{52}Cr [1–3], ^{164}Dy [4, 5] and ^{168}Er [6] magnetic atoms has been a giant step forward in the studies of quantum matter [7, 8]. BECs of magnetic atoms exhibit long-range dipole-dipole interaction (DDI) between atoms, depending on the mutual orientation of atomic magnetic moments [9], in addition to nonlinear effects induced by the s -wave contact interactions between the atoms, including repulsion and attraction. On the other hand, techniques based on the Feshbach resonance can efficiently control the contact nonlinearity [10], enabling the control of the interplay between the nonlocal (DDI) and local (contact) interactions for performing various manipulations with the dipolar BECs. In particular, this setting was elaborated in Ref. [11] to control spatial separation of spin-coupled BECs. In this regard, it is relevant to note that tunable long-range interatomic correlations can be induced by laser-induced DDIs in BECs [12], creating a *roton minimum* in the excitation spectrum, reminiscent of the well-known properties of the strongly correlated superfluid represented by liquid helium II [13, 14]. Rotons are also well known as elementary excitations in dipolar BECs, see [15]–[18] and references therein.

It is well known that the mean-field (MF) cubic self-attractions leads to the onset of the critical or supercritical collapse and eventual breakdown of the condensates, in the framework of the corresponding two- and three-dimensional (2D and 3D) Gross-Pitaevskii (GP) equations, respectively [19–22]. Therefore, it is relevant to search for physically relevant mechanisms that can stabilize 2D and 3D self-trapped modes, such as bright soli-

tons, solitary vortices, and others [23, 24]. In this context, beyond-MF effects, which have been the subject of intensive experimental investigations [25–27], have shown a great potential. In this vein, it was predicted [28, 29] that the full stability of 2D and 3D self-trapped states in a binary BEC, in the form of *quantum droplets* (QDs), may be provided by the Lee-Huang-Yang (LHY) corrections to the GP equations [30, 31], which represent the effect of quantum fluctuations around the MF state. This result follows a previous suggestion [32], made in the context of the three-body Efimov physics [33], which pointed out that the BEC system with attractive two-body interactions could eventually be stabilized against the collapse by a repulsive three-body term [34], leading to the formation of self-bound boson droplets, termed *boselets* in Ref. [32], so that a trapping potential is not needed to hold the particles together.

In terms of the corresponding GP formalism, the correction to the MF approximation, as considered in Ref. [28], is represented by quartic self-repulsion term, which is usually much weaker than the cubic MF one. The LHY correction becomes significant in the special case when the intraspecies self-repulsion and interspecies cross-attraction terms in the corresponding system of non-linearly coupled GP equations (mutuality fitted by means of the Feshbach resonance [35]) almost cancel each other for the symmetric state, with equal wave functions of the two components [28]. In particular, the “LHY superfluid” was predicted [36] and observed [37], in which the full cancellation of the MF fields makes the entire nonlinearity in the GP system represented solely by the LHY terms. In agreement with the predictions, the LHY corrections have made it possible to create robust QDs in binary BECs with the contact interactions [38–

42], as well as in dipolar condensates dominated by the long-range magnetic DDIs (see theoretical predictions in Refs. [43, 44] and experimental realizations in Refs. [45–47]). In the latter case, the interplay between long-range interactions and the LHY effect also makes it possible to realize supersolids in the dipolar quantum gases [48–50], see also review [51]. The effects of quantum fluctuations may support supersolids in other settings as well [52–57]. The role of the LHY corrections has also been demonstrated in experimental studies of the critical BEC temperature [58], quantum depletion [59], excitation spectrum [60], and thermodynamic equation of state [61]. It is relevant to mention that, when investigating the universality of the contact interactions in the regime of observable beyond-MF effects, no measurable contributions from three-body interactions were found [62].

Quantized vortices, first predicted in the framework of GP equations for trapped Bose gases in Ref. [63], have been created in experiments using rotating magnetic traps or applying laser stirring to BEC above a certain critical rotational frequency. The observation of the vortices provides compelling evidence for the occurrence of superfluidity in BECs, sharing some features with liquid helium [64]. In dipolar Bose gases, quantized vortices have been intensively investigated, within the MF approximation, in the last decades up to now [65–81]. The structure and stability of vortices in dipolar BECs are strongly affected by the anisotropy of the DDIs and their strengths, with respect to the contact interactions [65, 70, 71, 82, 83]. Static hydrodynamic solutions and their stability have been also explored for the rotating dipolar BECs in the Thomas-Fermi (TF) limit [84]. In this context, the structure of dipolar BECs was studied in the quasi-2D scenario with arbitrary orientations of the dipoles [73, 85]. The second-order-like phase transition of straight and helical vortex lines, occurring due to the effect of the dipoles' orientation, has also been reported [68]. DDI strongly affects the number, structure, and stability of vortices. Further, the critical rotational frequency for the nucleation of vortices decreases with the increase of the DDI strength, while the contact interactions enhance the vortex stability [74]. The stabilization of 2D and 3D self-trapped (localized) QDs with embedded vorticity due to the action of the LHY effect in the binary BECs with contact interactions were predicted, respectively, in Refs. [86] and [87]. On the other hand, the QD solutions for axially symmetric vortex states in the single-component dipolar BEC were found to be fully unstable [88].

Although experiments have been carried out with ^{164}Dy and ^{168}Er dipolar condensates by taking into account the effects of quantum fluctuations, quantized vortices in LHY-dominated superfluids have not yet been explored in detail. The recent experimental observation of quantized vortices in a dipolar condensate of lanthanide atoms [89, 90] motivates further theoretical studies and new experiments with single- and multi-vortex states in one-component and binary rotating condensates [11] in

the LHY-dominated regime. In light of the above, the main objective of the present paper is to report new results, based on systematic simulations, for the nucleation and dynamics of vortices in a one-component dipolar BEC in the LHY-dominated superfluid, featuring the interplay between dipolar and contact two-body interactions. The independent tunability of binary interactions and dipole-dipole interactions ensures that one may end up with a fluid completely dominated by quantum fluctuations alone.

The paper is organized as follows. In the next section, we formulate the single-component quasi-2D model including the DDI and LHY effect, basically following Ref. [11]. Systematic results, with the corresponding discussion, are reported in Section III. Section IV summarizes the paper with our main conclusions and perspectives.

II. THE GP SYSTEM WITH THE DDI AND LHY TERMS

We consider a dipolar atomic BEC of N atoms with mass m and magnetic dipole moment μ_M . The system is confined in a quasi-2D pancake-shaped harmonic oscillator trap,

$$V(\mathbf{r}) \equiv \frac{m\omega_{\perp}^2}{2} (x^2 + y^2 + \lambda^2 z^2), \quad (1)$$

with a fixed large aspect ratio, $\lambda \equiv \omega_z/\omega_{\perp} = 20$. In the rotating reference frame, the dynamics of the system is governed by the time-dependent GP equation for the wavefunction $\phi \equiv \phi(\mathbf{r}, t)$, which is subject to the unitary normalization [91–93]:

$$i\hbar \frac{\partial \phi}{\partial t} = \left[-\frac{\hbar^2}{2m} \nabla^2 + V(\mathbf{r}) - \Omega L_z + g_0 |\phi|^2 + g_{\text{LHY}} |\phi|^3 + \int U_{\text{dd}}(\mathbf{r} - \mathbf{r}') |\phi'|^2 d^3 \mathbf{r}' \right] \phi, \quad (2)$$

where $L_z \equiv -i\hbar(x\partial_y - y\partial_x)$ is the z -component of the angular momentum operator, with ΩL_z implying the rotation about the z -axis with angular frequency Ω . The coefficient g_0 of the cubic MF term is given in terms of the two-body s -wave scattering length a_s , as $g_0 = 4\pi\hbar^2 a_s N/m$. The DDI is represented by the integral term in Eq. (2), which refers to the quasi-2D geometry illustrated in Fig. 1 [9],

$$U_{\text{dd}}(\mathbf{r} - \mathbf{r}') \equiv \frac{\mu_0 \mu_M^2 N}{8\pi} \frac{(3 \cos^2 \varphi - 1)}{|\mathbf{r} - \mathbf{r}'|^3}. \quad (3)$$

The strength of the quartic nonlinear LHY term for the dipolar BEC is

$$g_{\text{LHY}} = \frac{64\hbar^2 \sqrt{\pi(a_s N)^5}}{m} \left(\frac{2}{3} + \varepsilon_{\text{dd}}^2 \right), \quad (4)$$

where $\varepsilon_{\text{dd}} \equiv a_{\text{dd}}/a_s$ is the ratio of the effective DDI scattering length,

$$a_{\text{dd}} \equiv \frac{m\mu_0\mu_M^2}{12\pi\hbar^2}, \quad (5)$$

and the s -wave two-body scattering length a_s [7].

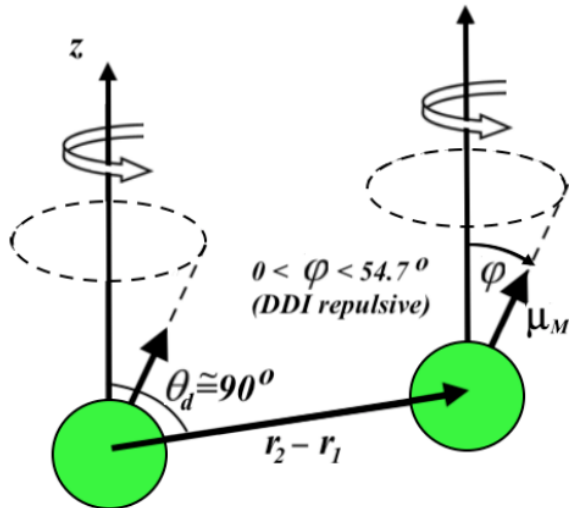


FIG. 1. The representation of DDIs in the dipolar quasi-2D BEC in the coordinate space. Angle between vector $\mathbf{r}_2 - \mathbf{r}_1$ and the z axis is $\theta_d \approx 90^\circ$. The variation of angle φ between the magnetic dipoles and the z axis alters the strength and sign of DDI, from repulsive to attractive.

A. DDI in the quasi-2D BEC

To define the DDI, we consider a pair of atoms placed at positions \mathbf{r} and \mathbf{r}' , with the respective vector $\mathbf{r} - \mathbf{r}'$ making angle θ_d with the z axis, so that $\theta_d \approx 90^\circ$ for the oblate (pancake-shaped) configuration. As shown in Fig. 1, the atoms have their magnetic moments polarized, by a polarizing magnetic field, in the same direction, making angle φ with the z axis. Similar to Refs. [9, 11], in the present case, the tunability of the DDI is provided by time-dependent polarizing fields, which set the magnetic moments in rapid rotation around the z axis. With the magnetic fields being a combination of the static (dc) component directed along the z axis and the rapidly rotating (ac) one in the (x, y) plane, one may neglect the motion of atoms driven by the ac field. With the time averaging performed over the rotation period, the corresponding 3D averaged DDI can be written in the scaled form as [9]

$$\langle V_{\text{3D}}^{(d)}(\mathbf{r} - \mathbf{r}') \rangle = \mu_0\mu_M^2 \left(\frac{3\cos^2\varphi - 1}{2} \right) \frac{1}{|\mathbf{r} - \mathbf{r}'|^3}, \quad (6)$$

where μ_0 is the free-space permeability, with the magnetic moment μ_M measured in units of the Bohr magneton μ_B . As said above, for the oblate configuration adopted here, with the condensate distributed in the (x, y) plane, we have $\theta_d \approx 90^\circ$, hence φ remains an appropriate angular coordinate for tuning the DDI strength, making it repulsive in the interval of $0 \leq \varphi < \varphi_{\text{magic}}$, and attractive for $\varphi_{\text{magic}} < \varphi \leq 90^\circ$, where $\varphi_{\text{magic}} \approx 54.7^\circ$ is the so-called “magic angle” [94]. DDI vanishes at $\varphi = \varphi_{\text{magic}}$, irrespective of the magnitude of the magnetic moment.

Equations (2) and (4) demonstrate that the short-range binary interaction, long-range DDI, and LHY correction are interdependent, which can impede the search for stable configurations, particularly vortices. Therefore, it may be helpful to develop a model exhibiting three independent interactions, which do not impact on each other. To this end, it is desirable to have the g_{LHY} coefficient which is affected not by the DDI orientation, but solely by the corresponding DDI scattering length (5). Therefore, a simple strategy to increase the impact of the LHY contribution is to assume a scenario in which one can adjust the contact and dipolar interactions, so that they effectively cancel out each other. To this aim, starting with a repulsive contact interaction, the long-range DDI should be tuned by adjusting the orientation angle φ in Fig. 1, making it attractive. Provided that the strength of the repulsive contact interaction is adjusted to stay within the possible range of the attractive DDI strength, it may be possible to identify the setting in which the LHY effect dominates the condensate. Similarly, with repulsive DDI, one can manipulate the contact interaction, tuning it to the attraction sign, again designing the LHY-controlled setting, with the dipole-dipole and contact MF interactions balancing each other.

Appropriate dimensionless parameters can be defined in terms of a reference frequency, which we set as $\omega_\perp = \omega_x = \omega_y$, see Eq. (1), and the corresponding oscillator length, $\ell_\perp = \sqrt{\hbar/(m\omega_\perp)}$. To cast Eq. (2) in the normalized form, we first rescale the time and coordinate variables as $\bar{t} \equiv \omega_\perp t$, $\bar{\mathbf{r}} \equiv \mathbf{r}$. Accordingly, we define $\bar{a}_s = a_s/\ell_\perp$, $\bar{a}_{\text{dd}} = a_{\text{dd}}/\ell_\perp$, with the wavefunction and system’s energy rescaled as $\bar{\phi} = \ell_\perp^{3/2}\phi$ and $\bar{E} = \hbar\omega_\perp E$. Next, we drop the overhead bars, assuming that all the variables and parameters are dimensionless. This transformation casts the GP equation (2) into the normalized form, with $\hbar = m = 1$ and redefined coefficients.

In our approach, we assume a strong harmonic trap confinement in the z -direction, allowing the 3D ground-state wavefunction be expressed by the ansatz $\phi(\mathbf{r}, t) \equiv (\lambda/\pi)^{1/4} \exp(-\lambda z^2/2) \psi(\boldsymbol{\rho}, t)$, where $\psi \equiv \psi(\boldsymbol{\rho}, t)$ is the effective 2D MF wavefunction in polar coordinates, where $\boldsymbol{\rho} \equiv (x, y) = (\rho \cos\theta, \rho \sin\theta)$. The factorized ansatz is substituted in Eq. (2), which is then multiplied by $\phi(z) \equiv (\lambda/\pi)^{1/4} \exp(-\lambda z^2/2)$ and integrated over z [95]. The corresponding procedure for the 2D reduction of the DDI term is elaborated in detail in Refs. [11, 75], in which the effective 2D DDI was de-

rived by applying the convolution theorem and using the 2D Fourier transform for the product of the DDI kernel and density, as $\int d\rho' V^{(d)}(\rho - \rho') |\psi(\rho')|^2 = \mathcal{F}_{2D}^{-1}[\tilde{V}^{(d)}(k_x, k_y) \tilde{n}(k_x, k_y)]$, where \mathcal{F}_{2D}^{-1} is the operator of the inverse Fourier transform. As a result, the DDI kernel can be expressed as the combination of two terms in the 2D momentum space, $\mathbf{k}_\rho = (k_x, k_y) = (k_\rho \cos \theta_k, k_\rho \sin \theta_k)$, for a fixed orientation φ of the magnetic dipoles (Fig. 1), accounting for the interactions perpendicular and parallel to the direction of the dipole moments:

$$\begin{aligned}\tilde{V}_\perp^{(d)}(k_x, k_y) &= 2 - 3\sqrt{\frac{\pi}{2\lambda}} k_\rho \exp\left(\frac{k_\rho^2}{2\lambda}\right) \operatorname{erfc}\left(\frac{k_\rho}{\sqrt{2\lambda}}\right), \\ \tilde{V}_\parallel^{(d)}(k_x, k_y) &= -1 + 3\frac{k_x^2}{k_\rho} \sqrt{\frac{\pi}{2\lambda}} \exp\left(\frac{k_\rho^2}{2\lambda}\right) \operatorname{erfc}\left(\frac{k_\rho}{\sqrt{2\lambda}}\right)\end{aligned}\quad (7)$$

where $\operatorname{erfc}(\xi)$ is the standard complementary error function. With all directions being possible in the (x, y) plane, the angular averaging amounts to $k_x^2 = k_\rho^2 \cos^2 \theta_k \rightarrow k_\rho^2/2$, so that the effective total 2D DDI kernel can be written in the momentum space as a function of k_ρ and φ , *viz.* $V_\varphi(k_\rho) \equiv \tilde{V}^{(d)}(k_x, k_y)$:

$$\begin{aligned}V_\varphi(k_\rho) &= \cos^2 \varphi \tilde{V}_\perp^{(d)}(k_x, k_y) + \sin^2 \varphi \tilde{V}_\parallel^{(d)}(k_x, k_y) \\ &= \frac{3 \cos^2 \varphi - 1}{2} \left[2 - 3\sqrt{\frac{\pi}{2\lambda}} k_\rho e^{\frac{k_\rho^2}{2\lambda}} \operatorname{erfc}\left(\frac{k_\rho}{\sqrt{2\lambda}}\right) \right].\end{aligned}\quad (8)$$

Thus, we have the effective GP equation given by

$$\begin{aligned}i \frac{\partial \psi}{\partial t} &= \left[-\frac{\nabla_\rho^2}{2} + \frac{\rho^2}{2} - \Omega L_z + g|\psi|^2 + \eta|\psi|^3 \right] \psi \\ &+ g_{dd}(\varphi) \int \frac{d^2 \mathbf{k}_\rho}{(2\pi)^2} e^{-i\mathbf{k}_\rho \cdot \boldsymbol{\rho}} \tilde{n}(\mathbf{k}_\rho, t) h_{2D}\left(\frac{k_\rho}{\sqrt{2\lambda}}\right) \psi,\end{aligned}\quad (9)$$

where $g_{dd}(\varphi) \equiv (g_{dd}/2)(3 \cos^2 \varphi - 1)$. Here, the coefficient η , which is defined below by Eq. (15), corresponds to the reduced LHY dimensionless coefficient g_{LHY} given by Eq. (4) for the dipolar system. The other factors in Eq. (9) are [96]

$$\begin{aligned}\tilde{n}(\mathbf{k}_\rho, t) &= \int d^2 \boldsymbol{\rho} e^{i\mathbf{k}_\rho \cdot \boldsymbol{\rho}} |\psi|^2, \\ h_{2D}(\xi) \Big|_{\xi \equiv \frac{k_\rho}{\sqrt{2\lambda}}} &= [2 - 3\sqrt{\pi} \xi \exp(\xi^2) \operatorname{erfc}(\xi)].\end{aligned}\quad (10)$$

The 2D GP equation (9) is elaborated for quasi-2D BEC in the next subsection. Further, in the framework of the quasi-2D approximation, the 3D two-body contact-interaction constant, g_0 , is replaced in Eq. (9) by the scaled one, $g \equiv \sqrt{8\pi\lambda} N a_s / \ell_\perp$. The rescaling transforms the original DDI coefficient $\mu_0 \mu_M^2 / (4\pi)$ into the dimensionless one, $g_{dd} = \sqrt{8\pi\lambda} N a_{dd} / \ell_\perp$, where a_{dd} is the DDI scattering length (5) [97]. One should note that the aspect ratio λ also appears explicitly in the integrated 2D expression for $V^{(d)}$ [11]. Considering the DDI tunability through the orientation angle φ of the magnetic moments, the DDI coefficient is written below as a function of φ , $g_{dd}(\varphi)$. For the length rescaling, an alternative is

to use the Bohr radius $a_0 (= 5.29 \times 10^{-11} \text{m})$, taking into account that $\ell_\perp = 10^{-6} \text{m} \approx 1.89 \times 10^4 a_0$.

The total energy corresponding to Eq. (9) can also be written as [98]

$$\begin{aligned}E &= \int dx dy \left\{ \frac{1}{2} [i\partial_x \psi - \Omega y \psi]^2 + [i\partial_y + \Omega x \psi]^2 \right. \\ &+ \frac{(1 - \Omega^2)(x^2 + y^2)}{2} |\psi|^2 + \frac{g}{2} |\psi|^4 + \frac{2}{5} \eta |\psi|^5 \left. \right\} \\ &+ \frac{g_{dd}(\varphi)}{2} \int \frac{d^2 \mathbf{k}_\rho}{(2\pi)^2} e^{-i\mathbf{k}_\rho \cdot \boldsymbol{\rho}} \tilde{n}(\mathbf{k}_\rho, t) h_{2D}\left(\frac{k_\rho}{\sqrt{2\lambda}}\right) |\psi|^2.\end{aligned}\quad (11)$$

In the limit of extremely tight confinement in the transverse direction, the effective nonlinearity in the LHY-amended GPE is different from the quartic term [29]. Nevertheless, one may use the 2D equations with the quartic term, such as Eq. (9), in relevant experimental settings with moderately tight confinement [99].

B. The LHY correction for the quasi-2D BEC

The LHY corrections can be taken into account in the usual MF 3D formalism similar to how it was done in Ref. [36], where the correction to the ground-state energy density of a homogeneous weakly repulsive Bose gas with contact interactions, is

$$\begin{aligned}\mathcal{E}_{\text{LHY}} &= \frac{\hbar^2}{15m} 256 \sqrt{\pi} (|a_s| n)^5 \\ &= \frac{\hbar \omega_\perp}{\ell_\perp^3} \frac{256 \sqrt{\pi}}{15} \left(N \frac{|a_s|}{\ell_\perp} |\psi(x, y)|^2 \sqrt{\frac{\lambda}{\pi}} e^{-\lambda z^2} \right)^{5/2}.\end{aligned}\quad (12)$$

The corresponding LHY corrections are given by

$$H_{\text{LHY}} \Psi = \left(\frac{128 \sqrt{\pi}}{3} \sqrt{\frac{N |a_s|^5}{\ell_\perp^5}} \right) |\psi(x, y)|^3 |\phi(z)|^3 \Psi. \quad (13)$$

Multiplying this term by the complex conjugate of $\phi(z)$, and integrating out the z -component, we obtain the following expression for the scaled LHY correction term,

$$H_{\text{LHY}} \psi = \frac{128}{3} \sqrt{\frac{2N^3}{5}} \left(\frac{\lambda^3}{\pi} \right)^{1/4} \left(\frac{|a_s|}{\ell_\perp} \right)^{5/2} |\psi|^3 \psi, \quad (14)$$

which provides the scaled coefficient corresponding to coefficient g_{LHY} in Eq. (4), in the absence of DDI. In the case of GP equation for the dipolar gas, the coefficient g_{LHY} needs to be multiplied by an additional factor, which depends on the DDI strength, as shown in Refs. [91–93, 100], thus giving rise to the interdependence between the LHY correction, contact interactions, and DDI. Including the DDI, we thus derive the effective coefficient for the scaled quasi-2D LHY correction as

$$\eta = \frac{64\sqrt{2}}{\sqrt{5}\sqrt{\pi}} \left(\sqrt{\lambda} N \right)^{\frac{3}{2}} \left(\frac{|a_s|}{\ell_\perp} \right)^{\frac{5}{2}} \left(\frac{2}{3} + \varepsilon_{dd}^2 \right). \quad (15)$$

It appears in Eq. (4), for a quasi-2D dipolar condensate with aspect-ratio parameter λ , that was defined above in Eq. (1).

C. The pure LHY nonlinearity in the quasi-2D GP equation

In the above derivation of Eq.(15) it is adopted that the dipoles are aligned in the same direction (Fig. 1), implying that the DDI is maximized at $\varphi = 0^\circ$ [91]. As also seen in Fig. 1, the effective DDI strength can be tuned by varying φ from 0 (maximum positive) to $\pi/2$ (maximum negative), being zero for $\varphi = \varphi_{\text{magic}}$. To take advantage of the tunability of DDI [9], we keep φ as an adjustable parameter. For this purpose, the LHY parameter (15) is redefined, as $\eta \equiv \eta(\varphi)$, with

$$\varepsilon_{\text{dd}} \equiv \varepsilon_{\text{dd}}(\varphi) \equiv \frac{a_{\text{dd}}}{a_s} \left(\frac{3 \cos^2 \varphi - 1}{2} \right). \quad (16)$$

Thus, the effective LHY coefficient is affected by two adjustable parameters: a_s and the angle φ . Independently of the signs of the contact and dipolar interactions, the LHY contribution is positive. The possibility to enhance the LHY contribution as compared with the main nonlinear terms, is to make use of both control parameters, so that one of the interactions is attractive, with the other being repulsive. The ideal condition for a pure LHY superfluid, is the overall total cancellation of the MF and dipolar terms. In the framework of a more realistic experimental setup, one can consider the situation in which we have an effective reduction of the two main nonlinear terms such that the fluid's nonlinearity is dominated by the quantum fluctuations. In the following section, we consider the ideal condition in which we can effectively remove the MF terms, *viz.*, DDI and contact ones, in Eqs. (9) and (11). The result is the following stationary 2D GP equation for the quantum superfluid (QS) with chemical potential μ_{QS} , and the respective energy per particle:

$$\begin{aligned} \mu_{\text{QS}}\psi &= \left[-\frac{1}{2}(\partial_x^2 + \partial_y^2) + \frac{x^2 + y^2}{2} - \Omega L_z + \eta(\varphi)|\psi|^3 \right] \psi, \\ E_{\text{QS}} &= \int dx dy \left\{ \frac{1}{2} [|i\partial_x - \Omega y \psi|^2 + |i\partial_y + \Omega x \psi|^2] \right. \\ &\quad \left. + \frac{(1 - \Omega^2)(x^2 + y^2)}{2} |\psi|^2 + \frac{2}{5} \eta(\varphi) |\psi|^5 \right\}. \end{aligned} \quad (17)$$

This possibility to effectively cancel the local and nonlocal MF nonlinear terms is somewhat similar to that proposed in Ref. [36], where a binary Bose mixture without DDI and rotation was considered, therefore our studies of on rotational properties of LHY superfluid, following below in section III C, may be accordingly applied to the setting addressed in Ref. [36]. In addition, it is relevant to mention that, for the 2D BEC trapped in the harmonic-oscillator potential, the critical rotational frequency Ω_c for a single vortex production has been analytically determined in Ref. [101], assuming the strong cubic nonlinearity obeying the Thomas-Fermi limit. In

the present notation, the corresponding expression is

$$\Omega_c \approx \frac{5}{2} \ln \left(0.67 \sqrt{2\mu} \right). \quad (18)$$

In the case of more general nonlinear interactions, such as the present case, which includes the DDI and LHY terms, the result is expected to be similar, as the essential differences originating from the nonlinear interactions, may be absorbed by the change of the chemical potential.

III. NUMERICAL RESULTS AND DISCUSSION

The main objective of this work is to explore the nucleation and dynamics of vortices in the BEC dominated by the LHY nonlinearity, assuming the effective mutual cancellation of the MF contact interactions and DDIs. In subsection A, the results are produced in the absence of the LHY term, aiming to verify the rotation effect in the usual situation, where the MF nonlinearity is taken into account. These results, which are consistent with previous investigations, serve as a benchmark for the comparison with the cases where the LHY term is the dominant one. In that subsection, the explicit dependence on the orientation angle φ is dropped in the DDI and LHY parameters, assuming that $\eta \equiv \eta(\varphi)$ is given by Eq. (16) and $g_{\text{dd}} \equiv g_{\text{dd}}(\varphi)$. Unless explicitly stated otherwise, this implies $\varphi = 0^\circ$. In particular, the pure LHY superfluid considered in subsection C relies on the assumption of the effective cancellation of the MF contact and DDI terms, making it relevant to keep the φ dependence of the coefficients η and g_{dd} .

A. Vortex modes in the absence of the LHY term

The numerical procedure to solve the 2D GP equation starts with the split-step Crank-Nicholson method. Its advantage is that the non-derivative nonlinear and linear terms can be treated very accurately, to secure the precision and robustness of the numerical scheme. In the present case, the usual split-step Crank-Nicholson method was combined with the fast Fourier transform approach, following the prescription given in Refs. [83, 95, 97]. Here, we have used a numerical code with 512×512 grid size, with spatial step sizes $\Delta x = \Delta y = 0.04$. The norm of the wave function is restored to be 1 at each time step $\Delta t = 0.01$.

The numerical results are exemplified by the vortex formation in two cases when the MF nonlinear terms in the GP equation represent the contact and dipolar interactions. The obtained results are consistent with previously reported ones, such as those for the rotating systems with the pure contact nonlinearity [63], and for the 3D dipolar rotating system with a high value of the aspect ratio [102]. Here, it is not only illustrative to consider these results, which are also useful to estimate effects produced by the MF terms in comparison to those produced by the LHY nonlinearity. For this purpose, we keep the same DDI and contact-interaction parameters throughout the present study. Figure 2 shows how the vortices emerge following the variation of the rotation frequency Ω in the usual nonlinear MF system, with $g = 100$, in the absence of the DDI and LHY terms ($g_{\text{dd}} = \eta = 0$) in Eq. (9). Consistent with the critical frequency (18) for the single vortex in the 2D BEC trapped in the harmonic-oscillator potential with frequency ω_\perp (where $\mu \approx 2.58$ is the

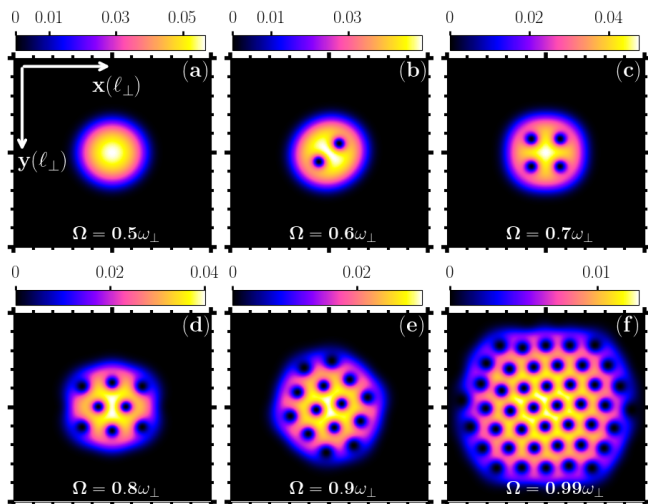


FIG. 2. (Color online) Density profiles $|\psi|^2$ projected onto the 2D plane, displaying vortex lattices with the nonlinearity represented solely by the MF contact interactions with $g = 100$. The rotation frequencies Ω (in units of ω_{\perp}) are indicated in the panels, with the density levels coded by the color bars. The x and y coordinates (in units of ℓ_{\perp}) cover the interval $[-10, +10]$.

scaled chemical potential), it is observed that the generation of vortices starts slightly below $\Omega \approx 0.6$, with the number of vortices N_v increasing almost linearly in the interval of $0.7 < \Omega < 0.9$. In Fig 3, our focus is on the generation of vortices with the nonlinearity represented solely by the DDI term, so that $(g, g_{dd}, \eta) = (0, 100, 0)$. Comparing the results displayed in Figs. 2 and 3, one can understand the efficiency of the respective parameters for the control of the production of vortices. These two cases, presented in Figs. 2 and 3, in the absence of the LHY nonlinearity, will be useful for comparison with the impact of the LHY term on the vortex production, which is the subject of the next subsection.

B. Vorticity in dipolar BEC with contact and LHY nonlinearities

The effect of LHY correction to the MF GP equation is estimated in this section by assuming $\eta = 200$ in Eq.(9), with $g = 100$ and without dipolar interactions. By strictly considering the expression (15), we should be aware that any specific value assumed for η will depend on a_s and a_{dd} . In particular, when $a_s = 0$, the quantum fluctuations become zero, such that $\eta \neq 0$ with $a_s = 0$ has no interest in our present analyses. However, we can verify rotational effects due to quantum fluctuation in a non-dipolar BEC system. For such a case, by assuming $g_{dd} = 0$ in Eq. (9), we first consider the results obtained in Fig. 2 with $g = 100$ to estimate how strong the parameter η of the quantum fluctuations could be assumed to reach some visible effect in the results. By looking for that, we have fixed $\eta = 200$ in our following studies, with the results being presented in Fig. 4. The quantum fluctuation contribution to the results, as expected, is quite small when compared with the MF nonlinear one, such that it starts to

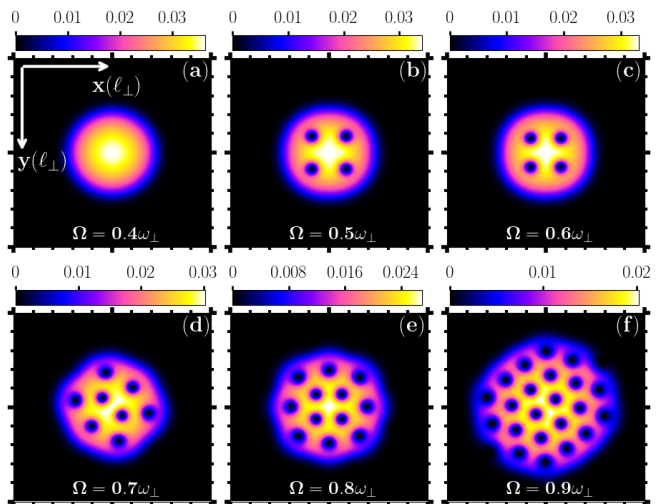


FIG. 3. (Color online) Density profiles $|\psi|^2$ projected onto the 2D plane, displaying vortex lattices with the nonlinearity represented solely by DDI with $g_{dd} = 100$. The rotation frequencies Ω are indicated in the panels, with the density levels coded by the color bars. The spatial domain and units are the same as in Fig. 2.

be noticeable only with $\eta = 200$ at Ω between 0.5 and 0.6. This can be verified in our results of Figs. 2 and 4. The effect of quantum fluctuations with such η can also be noticed for large rotations, close to $\Omega = 0.99$.

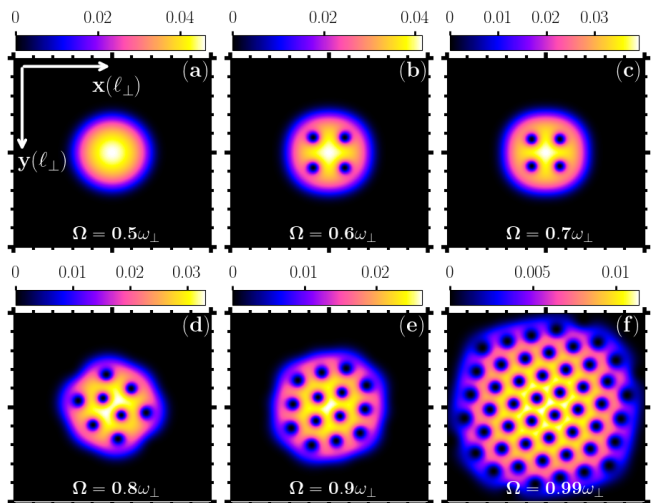


FIG. 4. (Color online) Density profiles $|\psi|^2$ projected onto the 2D plane, displaying vortex lattices with nonlinearity provided by contact and LHY interactions, with $g = 100$ and $\eta = 200$. The frequencies are indicated inside the panels, with the respective density levels given by color bars. The spatial domain and units are the same as in Fig. 2.

With the given results in Fig. 5, we are further verifying the significance of the LHY correction with $\eta = 200$. In this case, by considering both contact and dipolar nonlinearities

together with the quantum fluctuations, one should notice that LHY quantum fluctuation with $\eta = 200$ remains producing a small effect. The main change in the observed number of vortices in Fig. 5 is due to the cumulative effects related to contact and dipolar interactions, as compared with previous results shown in Figs. 2 and 3. Therefore, a possible way to enhance the effect of LHY correction, in comparison with other nonlinear effects, relies on playing with the signals of dipole-dipole and contact interactions, which can be performed by noticing that the strength of the LHY term, in the case of dipolar BECs, is only affected by the square of ε_{dd} , as shown by Eq. (16). Therefore, one can maximize or minimize the DDI effect just by controlling the φ dependence of η . This is being considered in the next section III C as a possible mechanism to generate a pure-LHY dipolar superfluid.

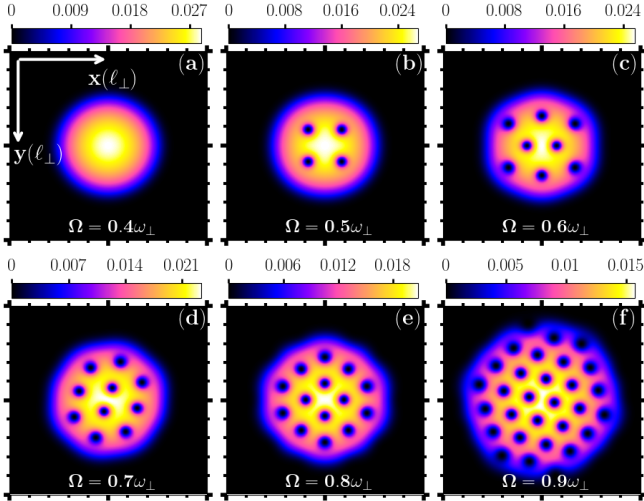


FIG. 5. (Color online) Density profiles $|\psi|^2$ projected onto the 2D plane, displaying vortex lattices with nonlinearity provided by contact, dipolar and LHY interactions, with $g = 100$, $g_{dd} = 100$, and $\eta = 200$. The frequencies are indicated inside the panels, with the respective density levels given by color bars. The spatial domain and units are the same as in Fig. 2.

C. The generation of vortices in the pure-LHY superfluid

The scenario where the LHY correction is the only source of the nonlinearity in the single-component dipolar BEC is explored in this subsection. It should be pointed out at this juncture that nonlinearity solely due to LHY was previously considered in the two-component BEC mixture with contact interactions [36, 37]. When the intra-species repulsion and inter-species attraction are precisely balanced, the MF contributions can be minimized or exactly canceled. To provide the approximate cancellation of the nonlinear MF local and nonlocal terms in the framework of the GP equation, we here consider the quasi-2D single-component dipolar BEC system introduced in the previous section. In this scenario, one can design the DDI intensity, by suitably adjusting the angle φ of the dipoles with respect to axis z (as represented in Fig. 1), and the contact interaction, through the scattering length a_s ,

by using the Feshbach resonance mechanism. Following that, within some approximation, we are left solely with the LHY nonlinearity, as postulated by Eq. (17), where the quintic term represents the LHY nonlinearity, with no explicit contribution from the contact and dipolar interactions.

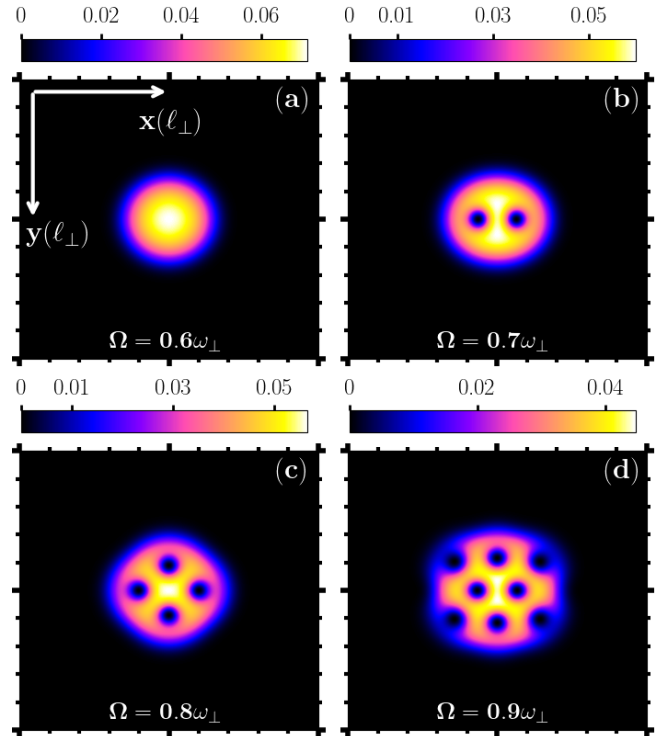


FIG. 6. (Color online) Density profiles $|\psi|^2$ projected onto the 2D plane, which display vortex lattices supported solely by the LHY nonlinearity, with $\eta = 200$ in Eq. (9). The rotation frequencies Ω are indicated in the panels, with the respective density levels defined by the color bars. The spatial domain and units are the same as in Fig. 2.

The rotating dipolar LHY superfluid is exemplified by setting $\eta = 200$ in Eq. (17). For this dipolar BEC system, the values of a_s and a_{dd} , which are included in expression (15), are not critical, provided that they are tuned to secure the approximate cancellation of the local and nonlocal MF terms. By changing the rotation frequency Ω from 0, by increments of $\Delta\Omega = 0.1$, we have observed no vortex produced for $\Omega \leq 0.6$ (in units of ω_\perp), with a pair of vortices being verified at $\Omega = 0.7$. Next, two and four pairs ($N_v = 4$ and 8) are observed at $\Omega = 0.8$ and $\Omega = 0.9$, respectively. These results are shown in Fig. 6. In more detail, we explored the values of Ω to produce the first four vortices, with results for the density plots and corresponding phases presented in Fig. 7. The phase map uses a color scale from $-\pi$ to $+\pi$, determined by the $\arctan(\text{Im}\psi/\text{Re}\psi)$. Beyond the trap boundaries, the phase is a numerical artifact, which arises from densities that are numerically small but not vanish.

As observed by the Ω values indicated in the four panels of Fig. 7, particularly in the cases to produce one and three stable vortices, careful fine tuning of Ω was required, with the values of Ω being, respectively, 0.6401 and 0.768. These findings reveal criticality in the states concerning Ω , for relatively

small number of produced vortices, N_v . More explicitly, at $\Omega = 0.6400$, no vortex can be found, whereas two vortices are generated at $0.6410 \leq \Omega \leq 0.767$, as shown in Fig. 7(b). Next, by slightly increasing the rotation frequency to $\Omega = 0.768$, a state with three-vortex is obtained, which persists in a very narrow interval, $0.768 \leq \Omega \leq 0.778$. A small variation in Ω can transform the three-vortex state into a two- or four-vortex one (at $\Omega \leq 0.767$ and $\Omega \geq 0.779$, respectively). The four-vortex state is produced in a broader interval, $0.779 \leq \Omega \leq 0.881$, with Fig. 8(d) displaying the result for $\Omega = 0.779$. This behavior, with vortex configurations being more stable with 2 and 4 vortices than with 1 and 3 vortices, is apparently a characteristic of the pure LHY superfluid in our quasi-2D approach, which is represented by the quartic nonlinearity in the GP equation with a strong pancake-like aspect ratio.

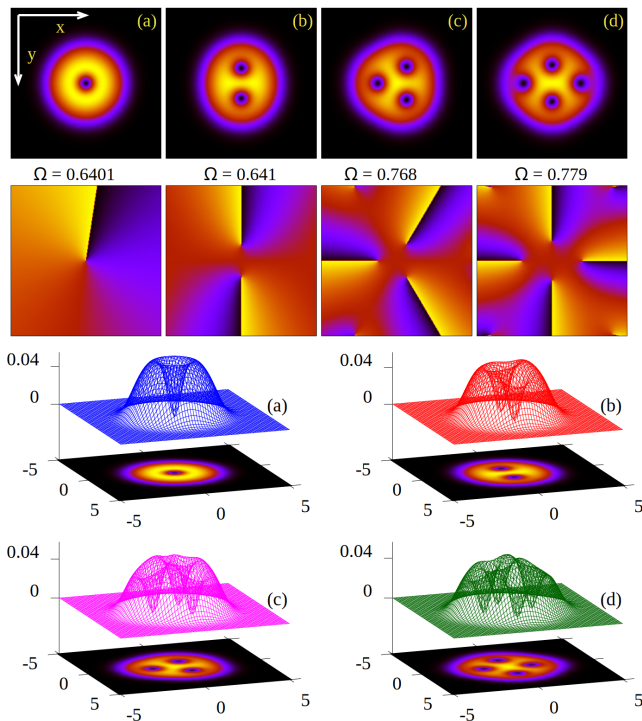


FIG. 7. (Color online) For the LHY superfluid with $\eta = 200$ at four values of Ω (in units ω_\perp), the density profiles $|\psi|^2$ shown in the first row with the respective phases patterns shown in second row while the corresponding 3D representations drawn in the lower rows of the figure. Panel (a) pertains to the critical frequency, $\Omega_c = 0.6401$, for the creation of the single-vortex configuration. The phase color map (the second row) spans from $-\pi$ (darkest blue) to $+\pi$ (brightest yellow), encircling each singularity in a clockwise direction, with zero value denoted by the maximum-red color.

Our results for the pure-LHY nonlinearity are consistent with results reported in Ref. [63], in which only the contact interactions have been considered, and the predictions were produced for rotating states within a more general 3D framework. For the first four stable vortices shown in Figs. 7, with $\Omega = 0.6401, 0.641, 0.768$, and 0.779 , the respective values of the system-averaged angular momentum per particle is $\langle L_z \rangle = 1, 1.75, 2.35$ and 2.85 . These results are analyzed in Fig. 8, considering the respective time evolution of $\langle L_z \rangle$. Fig.

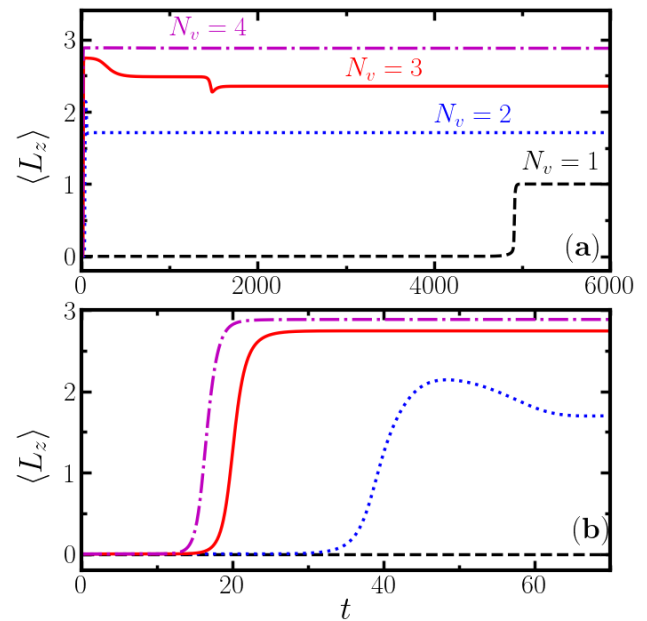


FIG. 8. (Color online) In the case when the nonlinearity is represented solely by the LHY term, we show the long-time evolution of the angular momentum $\langle L_z \rangle$ (in units of \hbar), corresponding to the production of one to four vortices, as indicated in panel (a). In panel (b) we display the same case as in (a) for a much shorter time interval, $t < 70$ (in units ω_\perp^{-1}). The respective values for the rotation velocity Ω are given in the caption of Fig. 7. The four established values, $\langle L_z \rangle = 1, 1.75, 2.35$, and 2.85 , agree with the ones reported in Ref. [63] for the case of pure contact interactions.

ure 8 shows how far one needs to evolve $\langle L_z \rangle$ to obtain stable vortex states. In addition, as the single-vortex configuration shown in (a₁) of Fig. 7 can only be obtained after fine-tuning the rotational frequency within four decimal digits, we can identify the critical rotation frequency for the production of a single vortex in the pure-LHY case as $\Omega_c = 0.6401$. The corresponding numerical value of the chemical potential is $\mu_{QS} = 1.78$. This result is close enough to the one that can be extracted from the TF relation (18), $\mu \approx 1.86$, for the same Ω_c .

Usually, the vortex patterns are made energetically preferable states with the help of the trap symmetry and boundary conditions. As shown in Refs. [63, 103, 104], for contact interactions, the critical rotation frequencies Ω_{cn} , which are necessary to attain stable states with n vortices are determined by the MF two-body interaction. Therefore, for vortices supported by the pure LHY nonlinearity, such critical frequencies and the corresponding stability may be estimated by means of the respective coefficient η , given in Eq. (15).

Figure 9 summarizes the results for N_v versus Ω , varying Ω up to 0.99, for the solely-LHY nonlinearity, with strength $\eta = 200$. In this case, the largest number of vortices found for $\Omega = 0.99$ is $N_v = 20$. The figure displays the range intervals of frequencies $\Delta\Omega$ for the given specific values of N_v . Notable are the cases with $N_v = 2, 4$ and 8 , which have larger $\Delta\Omega$ than the other cases. Also, noticeable is the case with $N_v = 1$, which has $\Omega_c = 0.6401$ with $\Delta\Omega < 0.001$ (In this regard, see also the upper row of Fig.7). Inside Fig. 9, we have also included

density plots obtained for $N_v = 5, 6, 7$ and 10 , to complement the ones previously shown for $N_v \leq 4$.

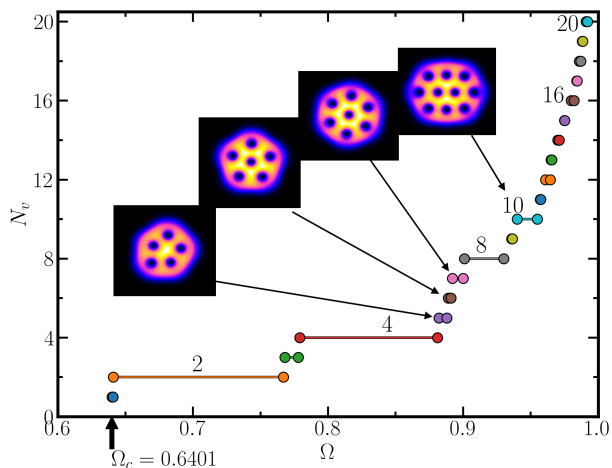


FIG. 9. The dependence of the number of vortices, N_v , on the rotation frequency Ω (in units of ω_\perp) for the pure LHY case, with $\eta = 200$ (see Eq. (15)). The position of the single-vortex critical frequency, $\Omega_c = 0.6401$, is indicated. For even numbers $N_v \geq 2$, the existence ranges of Ω are indicated too. The density profiles for $N_v = 5, 6, 7$, and 10 are plotted in the panel.

D. The effect of the rotational frequency

For the usual BEC system trapped in the harmonic oscillator potential, with the cubic MF nonlinearity, the rotating states were first predicted in Ref. [63] in the framework of a more general 3D framework, considering the generation of vortices, with the corresponding angular momentum being a function of the rotation velocity Ω . The previous section, confirms the occurrence of the same kind of vortex-generating mechanism in the LHY-dominated condensate, as in the case of the one with the MF nonlinearity. By adding the rotation to the system, all vortices are produced with the same vorticity sign, without vortex-antivortex annihilation.

The findings for the vortex configurations are summarized in Table I for all five nonlinearity cases that we have considered. In the table, we report the numerical results obtained for the chemical potential, total energy per particle E , and number of visible vortices N_v , for specific values of the rotation frequency Ω , which are given with one decimal digit. For the five cases being considered, the corresponding behaviors of E and μ , as functions of Ω , are presented in two panels of Fig. 10. The energy cost of generating vortices can be verified from the results provided in Table I. In particular, by focusing on case V of the table, where we have only the LHY nonlinear term, the energy cost of producing a pair of vortices, as compared with the non-rotating case ($E_{\Omega=0}$), is $\approx 22\%$ at $\Omega = 0.7$. On the other hand, when we have only the MF contact nonlinearity (column I in the table), the cost is $\approx 14\%$ at $\Omega = 0.6$. This indicates that the vortices are more likely to be produced in the presence of the pure MF contact nonlinearity than in the case of the pure LHY nonlinearity.

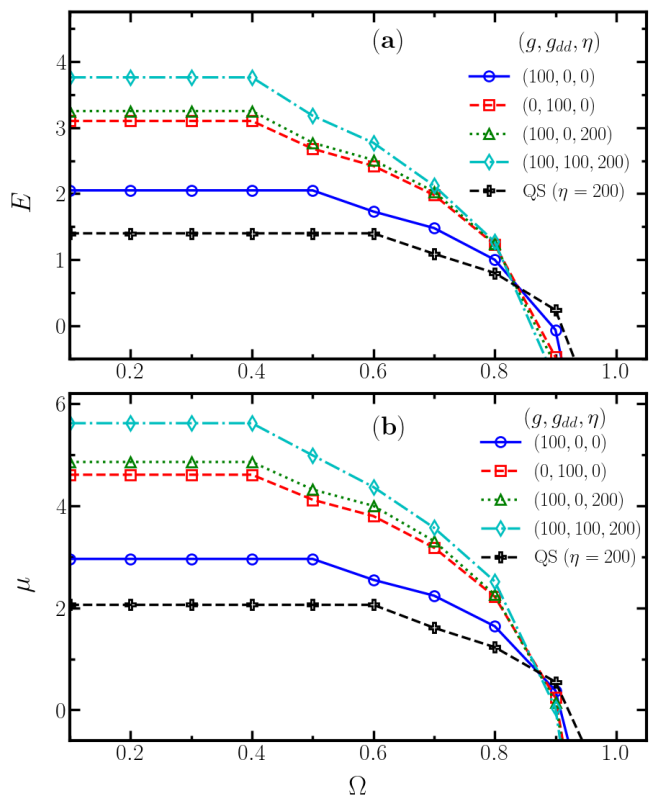


FIG. 10. (Color online) Energy E per particle (a) and the corresponding chemical potential μ (b) are shown as functions of Ω , for five different combinations of the interactions considered in Table I (as indicated in the panels). The energy and frequency units are, respectively, $\hbar\omega_\perp$ and ω_\perp .

Similarly, as shown in Ref. [101] for the contact MF non-linear interaction, the critical frequency necessary to produce the first vortex is given by the approximate analytical expression (18). Essentially, such an approximate expression in terms of the chemical potential is expected to be similar for all five cases considered in Table I. Given the exact numerical results for $\mu(\Omega)$, when starting to deviate from the no-rotation case, $\mu(\Omega = 0)$, we can obtain the corresponding single-vortex critical frequencies. Roughly, these critical frequencies can be numerically extracted from the results provided in Fig. 10, as well as from Table I.

Figure 11 summarizes the relationship between the angular momentum per particle and the number of vortices N_v . The data exhibit a clear linear trend, in excellent agreement with the Feynman's prediction for the angular momentum in a rapidly rotating superfluid [13]. The vortex core (where the density is zero) is a nodal line of the wave function. Preventing the kinetic energy from diverging, the core provides a cutoff, with a radius on the order of the healing length $\xi = \hbar/\sqrt{2mng_{eff}}$, where g_{eff} is the effective interaction strength. Next, we briefly discuss how the different kind of nonlinear interactions affect the corresponding healing lengths.

TABLE I. The effect of rotation frequency Ω on chemical potential (μ), total energy per particle (E), number of visible vortices (N_v), and angular momentum per particle, $\langle L_z \rangle$ for five different sets of parameters considered in this work. Case I (the pure MF contact interaction, with $g = 100$); case II (the pure DDI, with $g_{dd} = 100$); case III (with the contact-MF and LHY terms, without DDI, for $g = 100$ and $\eta = 200$); case IV (the nonzero contact-MF, DDI, and LHY terms, with $g = 100$, $g_{dd} = 100$, and $\eta = 200$); and case V (the pure LHY nonlinearity, with $\eta = 200$). In the pure-LHY superfluid, one should observe that the critical frequencies Ω_c for producing one and two vortex states are about the same within two decimal digits (being, respectively, 0.6401 and 0.6410). It implies that a single-vortex production is numerically quite challenging. In this table, the corresponding values for $N_v = 1$ are: $\Omega = 0.6401$, $\mu = 1.78$, $E = 1.21$, and $\langle L_z \rangle = 1$.

Ω	μ ($\hbar\omega_\perp$)					E ($\hbar\omega_\perp$)					N_v					$\langle L_z \rangle$ (\hbar)				
	I	II	III	IV	V	I	II	III	IV	V	I	II	III	IV	V	I	II	III	IV	V
0.0	2.96	4.61	3.40	5.62	2.06	2.05	3.10	2.30	3.76	1.40	0	0	0	0	0	0	0	0	0	0
0.4	2.96	4.61	3.40	5.62	2.06	2.05	3.10	2.30	3.76	1.40	0	0	0	0	0	0	0	0	0	0
0.5	2.96	4.12	3.40	4.99	2.06	2.05	2.68	2.30	3.18	1.40	0	4	0	4	0	0	2.76	0	2.99	0
0.6	2.59	3.80	2.83	4.37	2.06	1.76	2.42	1.84	2.77	1.40	2	4	4	8	0	1.69	3.06	2.72	4.68	0
0.7	2.24	3.07	2.50	3.54	1.61	1.48	1.89	1.58	2.16	1.09	4	8	4	10	2	2.85	4.91	3.05	6.13	1.71
0.8	1.62	2.22	1.69	2.51	1.23	0.99	1.23	0.96	1.26	0.80	8	12	8	14	4	4.34	6.98	5.00	8.44	2.88
0.9	0.38	0.24	0.47	0.04	0.55	-0.05	-0.47	-0.07	-0.03	0.24	14	22	14	28	8	7.19	11.38	8.10	14.12	4.53
0.99	-3.81	-6.06	-4.30	-7.37	-1.79	-3.99	-6.37	-4.51	-7.76	-1.89	42	68	48	80	20	20.75	30.94	22.73	36.53	11.99

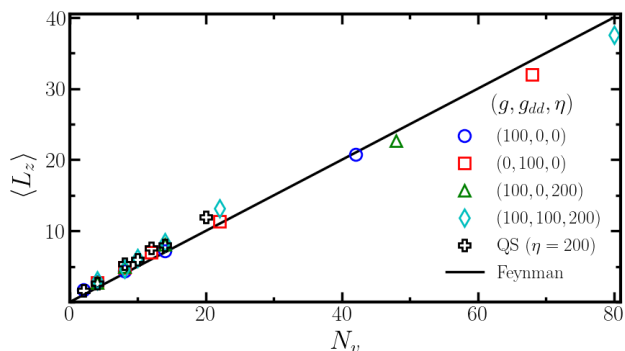


FIG. 11. (Color online) The linear increase of the angular momentum per particle $\langle L_z \rangle$ (in units of \hbar), associated with the change in the number of vortices, N_v , is confirmed for all the cases presented in Table I. As shown, the results are close to the linear behavior (solid line) predicted by Feynman [13]. The parameters are indicated in the panel, where QS stands for the solutions corresponding to Eq. (17), pertaining to the pure-LHY nonlinearity.

E. The healing length in the LHY-corrected case

From the density results presented in Figs. 2 and 6-7, by comparing cases with identical numbers of vortices, one can verify that the vortex healing lengths (radial sizes) slightly increase when proceeding from the usual cubic (pure contact) to the pure quartic LHY nonlinearity in the GP formalism. We can estimate the healing lengths more precisely using the results in Table I. As shown in Appendix A, the full-dimensional healing length for the LHY-corrected case is given by $\xi = \hbar / \sqrt{2m \left(g_0 n_0 + \frac{3}{2} g_{LHY} n_0^{3/2} \right)}$, where n_0 is the equilibrium bulk density. So, for the usual MF, we have $\xi_{MF} = \hbar / \sqrt{2m (g_0 n_0)} = \hbar / \sqrt{2m \mu_{MF}}$; whereas, for pure LHY interaction, $\xi_{LHY} = \hbar / \sqrt{3m g_{LHY} n_0^{3/2}} = \hbar / \sqrt{3m \mu_{LHY}}$. Us-

ing the dimensionless chemical potentials from Table I, we next compare the four-vortex configurations, where the vorticity is the most stable. For the pure contact interaction: $\Omega = 0.7$ (Fig. 2c), with $\mu_{MF} \approx 2.24$; and, for the pure LHY, $\Omega = 0.8$ (Fig. 6c), with $\mu_{LHY} \approx 1.23$. Therefore, $\xi_{LHY} / \xi_{MF} \approx \sqrt{2\mu_{MF} / (3\mu_{LHY})} \approx 1.10$, which indicates that the vortices in pure LHY quantum fluids have healing lengths about 10% larger than for the cases with only contact interactions. With the healing length slightly larger in the LHY fluid, the space between the radial borders of the vortices will be reduced accordingly. The intervortex distance (between the central cores), as shown in Ref. [105], is given by $l_\Omega = \sqrt{\hbar / (m\Omega)}$, which depends on the rotational frequency, consistent with the Feynman's prediction [13]. Therefore, when comparing cases having the same number of vortices but different nonlinearities, this intervortex distance should be slightly changed according to the changes of the rotational frequency. In our example of four vortices, the estimated distance between vortices is $l_{\Omega_{LHY}} / l_{\Omega_{MF}} \approx \sqrt{7/8} \approx 0.935$.

IV. CONCLUSION

In the present work, considering the rotating dipolar BEC, we investigate the impact of quantum fluctuations, represented by the LHY correction to the GP equation, on the formation and dynamics of individual vortices and vortex lattices. The main outcome of our analysis is related to the scenario of vortex production when the only source of nonlinearity is provided by the LHY term. This condition may approximately hold for the single-component dipolar BEC, with the mean-field (MF) contact interaction and DDI (dipole-dipole interaction) roughly canceling each other. To achieve this setting, one has to select appropriate values of the strengths of the MF contact and dipole-dipole interactions, which can be provided through the Feshbach resonance, and by adjusting the angle that determines the orientation of the atomic magnetic moments. It is shown that the LHY-only nonlinearity can be made strong enough to produce vortices in the

dipolar superfluid. For the smaller numbers of stable vortices ($N_v \leq 5$), it being more likely to obtain even rather than odd numbers of vortices when varying the rotational frequency Ω . This means that the range of Ω is relatively large to generate even numbers (2 or 4) of the vortices, being much smaller for the odd numbers (1 and 3). This feature is particularly pronounced in the pure LHY case, so that, for the single-vortex case, the corresponding range of the rotation frequency Ω is so narrow that it can be identified with the critical one Ω_c for the production of the single vortex. This effect, related to the quartic LHY nonlinearity, can also be partially attributed to the aspect ratio of the 3D trap. In a less pronounced form, a similar effect was also noted for the relatively small values of vortices in the case of pure MF contact interactions. A more detailed investigation related to this effect, considering different parametrization, may be required to clarify the role of the aspect ratio and its interplay with the nonlinearity.

We have also computed, within the framework of our quasi-2D model, the number of vortices, chemical potential, and energy per particle, expressed as functions of the rotation frequency Ω . For that purpose, we have considered specific combinations of the strengths of the MF contact interaction, DDI, and LHY nonlinearity. These parameters are assumed to be large enough to study the vortex production from the perspective of possible experimental realizations in dipolar BEC systems. The results demonstrate that, while the vortex numbers consistently increase with the growth of Ω , the chemical potential and energy decrease. From this study, when considering the pure LHY nonlinearity, exemplified by a particular value of the strength, which can be further generalized, we conclude how to precisely identify the single-vortex critical frequency, along with the corresponding values of the chemical potential and energy. In all the investigated cases, we have observed results consistent with Feynman's prediction of a linear dependence between angular momentum per particle and the number of vortices. Finally, we briefly discuss the vortex distribution and corresponding healing lengths in a trap in view of the different kinds of nonlinearities, by confronting the case with pure MF, with that one with pure LHY quantum fluid, with rotations such that the same number of vortices is produced. The results are consistent with experimental observations that $\xi_{LHY} > \xi_{MF}$.

ACKNOWLEDGMENTS

S.S. thanks Fundação de Amparo à Pesquisa do Estado de São Paulo (FAPESP) for the fellowship support, Proj. 2024/04174-8. R.R. wishes to acknowledge the financial assistance from DST-CURIE(DST-CURIE/PG/54) and ANRF(CRG/2023/008153) L.T. also acknowledges partial support from FAPESP (Proj. 2024/01533-7) and Conselho Nacional de Desenvolvimento Científico e Tecnológico (Proc. 303263/2025-3). The work of B.A.M. was supported, in part, by the Israel Science Foundation, through grant No. 1695/22.

APPENDIX: THE HEALING LENGTH OF A VORTEX IN AN LHY-CORRECTED SUPERFLUID

The healing length for a vortex in an LHY-corrected superfluid is defined by the linearized density recovery around the bulk equilibrium, governed by an effective coupling g_{eff} , that includes the derivative of the LHY term with respect to density. In view of our purpose, to simplify this appendix, we consider a non-dipolar system. The density is zero at the core of the vortex and heals to the equilibrium density $n_0 \equiv |\psi_0(\mathbf{r})|^2$ as going away from it. This equilibrium density itself is determined by balancing the MF (with interaction g_0) and LHY (with interaction strength g_{LHY}) pressures in the bulk, often leading to a flat-top droplet if the confinement is weak. By ignoring the external potential, considering uniform gas bulk equilibrium condition, the pressure balance gives

$$\mu_0 = g_0 n_0 + g_{LHY} n_0^{3/2}. \quad (\text{A1})$$

For a stationary straight vortex line with winding number one, using the ansatz $\psi(\mathbf{r}) = \sqrt{n(r)}e^{i\varphi}$, with r being the distance from the core, the real part of the extended GP equation is

$$-\frac{\hbar^2}{2m} \left[\frac{1}{r\sqrt{n}} \frac{d}{dr} \left(r \frac{d\sqrt{n}}{dr} \right) - \frac{1}{r^2} \right] + g_0 n + g_{LHY} n^{3/2} = \mu_0. \quad (\text{A2})$$

At $r \rightarrow \infty$, $n \rightarrow n_0$, with small density deviations being $\delta n = n_0 - n$, the linearization yields the healing length. The effective nonlinearity is now $g_0 n + g_{LHY} n^{3/2}$. By expanding the chemical potential about n_0 , we have

$$\mu(n) \approx \mu_0 + \left(g_0 + \frac{3}{2} g_{LHY} n_0^{1/2} \right) (n - n_0), \quad (\text{A3})$$

such that the effective coupling strength governing the stiffness against density variations is

$$g_{eff} = g_0 + \frac{3}{2} g_{LHY} n_0^{1/2}. \quad (\text{A4})$$

For a self-bound droplet, where g_0 can be negative, but g_{eff} is positive and nonsmall, the LHY term provides the dominant repulsion stabilizing the core. In analogy with the standard formalism, the healing length of a vortex in an LHY-corrected superfluid is given by

$$\xi = \frac{\hbar}{\sqrt{2m g_{eff} n_0}} = \frac{\hbar}{\sqrt{2m \left(g_0 + \frac{3}{2} g_{LHY} n_0^{1/2} \right) n_0}}. \quad (\text{A5})$$

Therefore, in a regime dominated by the LHY term (the droplet regime), assuming $g_0 = 0$, we obtain the healing length, as

$$\xi_{LHY} \approx \frac{\hbar}{\sqrt{3m g_{LHY} n_0^{3/2}}} = \frac{\hbar}{\sqrt{3m \mu_{LHY}}}, \quad (\text{A6})$$

which scales with the bulk density as $n_0^{-3/4}$, different from the MF scaling $\sim n_0^{-1/2}$. In terms of the respective chemical potentials, the factor $1/\sqrt{2}$ is replaced by $1/\sqrt{3}$.

-
- [1] A. Griesmaier, J. Stuhler, T. Koch, M. Fattori, T. Pfau, and S. Giovanazzi, Comparing contact and dipolar interactions in a Bose-Einstein condensate, *Phys. Rev. Lett.* **97**, 250402 (2006).
- [2] T. Lahaye, T. Koch, B. Fröhlich, M. Fattori, J. Metz, A. Griesmaier, S. Giovanazzi and T. Pfau, Strong dipolar effects in a quantum ferrofluid, *Nature* **448**, 672 (2007).
- [3] T. Koch, T. Lahaye, J. Metz, B. Fröhlich, A. Griesmaier and T. Pfau, Stabilization of a purely dipolar quantum gas against collapse, *Nature Phys.* **4**, 218 (2008).
- [4] S. H. Youn, M. Lu, U. Ray, and B. L. Lev, Dysprosium magneto-optical traps, *Phys. Rev. A* **82**, 043425 (2010).
- [5] M. Lu, N. Q. Burdick, S. H. Youn, and B. L. Lev, Strongly dipolar Bose-Einstein condensate of dysprosium, *Phys. Rev. Lett.* **107**, 190401 (2011).
- [6] K. Aikawa, A. Frisch, M. Mark, S. Baier, A. Rietzler, R. Grimm, and F. Ferlaino, Bose-Einstein condensation of erbium, *Phys. Rev. Lett.* **108**, 210401 (2012).
- [7] T. Lahaye, C. Menotti, L. Santos, M. Lewenstein, T. Pfau, The physics of dipolar bosonic quantum gases, *Rep. Prog. Phys.* **72**, 126401 (2009).
- [8] M. A. Baranov, M. Dalmonte, G. Pupillo, and P. Zoller, Condensed matter theory of dipolar quantum gases *Chem. Rev.* **112**, 5012 (2012).
- [9] S. Giovanazzi, A. Görlitz, and T. Pfau, Tuning the dipolar interaction in quantum gases, *Phys. Rev. Lett.* **89**, 130401 (2002).
- [10] C. Chin, R. Grimm, P. Julienne, and E. Tiesinga, Feshbach resonances in ultracold gases, *Rev. Mod. Phys.* **82**, 1225 (2010).
- [11] R. K. Kumar, L. Tomio, and A. Gammal, Spatial separation of rotating binary Bose-Einstein condensates by tuning the dipolar interactions, *Phys. Rev. A* **99**, 043606 (2019).
- [12] D. H. J. O'Dell, S. Giovanazzi and G. Kurizki, Rotons in gaseous Bose-Einstein condensates irradiated by a laser, *Phys. Rev. Lett.* **90**, 110402 (2003).
- [13] R. P. Feynman, in *Progress in Low Temperature Physics* vol 1, ed. C. J. Gorter (Amsterdam: North-Holland, 1955) p 17.
- [14] P. Nozière, Is the roton in superfluid 4He the ghost of a Bragg spot?, *J. Low Temp. Phys.* **137**, 45-67 (2004).
- [15] L. Santos, G. V. Shlyapnikov, and M. Lewenstein, Roton-Maxon Spectrum and Stability of Trapped Dipolar Bose-Einstein Condensates, *Phys. Rev. Lett.* **90**, 250403 (2003).
- [16] U. R. Fischer, Stability of quasi-two-dimensional Bose-Einstein condensates with dominant dipole-dipole interactions, *Phys. Rev. A* **73**, 031602(R) (2006).
- [17] C. Ticknor, R. M. Wilson, and J. L. Bohn, Anisotropic Superfluidity in a Dipolar Bose Gas, *Phys. Rev. Lett.* **106**, 065301 (2011).
- [18] A. Villois, M. Onorato, and D. Proment, Vortex to Rotons Transition in Dipolar Bose-Einstein Condensates, *Phys. Rev. Lett.* **124**, 253401 (2025).
- [19] L. Bergé, Wave collapse in physics: principles and applications to light and plasma waves, *Phys. Rep.* **303**, 259 (1998).
- [20] C. Sulem and P.-L. Sulem, *The nonlinear Schrödinger equation: Self-Focusing and wave collapse* (Springer, New York, 1999).
- [21] A. Gammal, T. Frederico, and L. Tomio, Critical number of atoms for attractive Bose-Einstein condensates with cylindrically symmetrical traps, *Phys. Rev. A* **64**, 055602 (2001).
- [22] G. Fibich, *The nonlinear Schrödinger equation: Singular solutions and optical collapse* (Springer, Heidelberg, 2015).
- [23] Y. V. Kartashov, L. Torner, M. Modugno, E. Ya. Sherman, B. A. Malomed and V. V. Konotop, Multidimensional hybrid Bose-Einstein condensates stabilized by lower-dimensional spin-orbit coupling *Phys. Rev. Res.* **2**, 013036 (2020).
- [24] B. A. Malomed, *Multidimensional Solitons* (AIP Publishing, Melville, New York, 2022).
- [25] A. Altmeyer, S. Riedl, C. Kohstall, M. J. Wright, R. Geursen, M. Bartenstein, C. Chin, J. H. Denschlag, and R. Grimm, Precision measurements of collective oscillations in the BEC-BCS crossover, *Phys. Rev. Lett.* **98**, 040401 (2007).
- [26] Y.-i. Shin, A. Schirotzek, C. H. Schunck, and W. Ketterle, Realization of a strongly interacting Bose-Fermi mixture from a two-component Fermi gas, *Phys. Rev. Lett.* **101**, 070404 (2008).
- [27] S. B. Papp, J. M. Pino, R. J. Wild, S. Ronen, C. E. Wieman, D. S. Jin, and E. A. Cornell, Bragg spectroscopy of a strongly interacting ^{85}Rb Bose-Einstein condensate, *Phys. Rev. Lett.* **101**, 135301 (2008).
- [28] D. S. Petrov, Quantum mechanical stabilization of a collapsing Bose-Bose mixture, *Phys. Rev. Lett.* **115**, 155302 (2015).
- [29] D. S. Petrov and G. E. Astrakharchik, Ultradilute low-dimensional liquids, *Phys. Rev. Lett.* **117**, 100401 (2016).
- [30] T. D. Lee and C. Yang, Many-Body problem in quantum mechanics and quantum statistical mechanics, *Phys. Rev.* **105**, 1119 (1957).
- [31] T. D. Lee, K. Huang, and C. N. Yang, Eigenvalues and eigenfunctions of a Bose system of hard Spheres and its low-temperature properties, *Phys. Rev.* **106**, 1135 (1957).
- [32] A. Bulgac, Dilute quantum droplets, *Phys. Rev. Lett.* **89**, 050402 (2002).
- [33] V. Efimov, Energy levels of three resonantly interacting particles, *Nucl. Phys. A* **210**, 157 (1973).
- [34] A. Gammal, T. Frederico, L. Tomio and Ph. Chomaz, Atomic Bose-Einstein condensation with three-body interactions and collective excitations, *J. Phys. B: At. Mol. Opt. Phys.* **33**, 4053 (2000).
- [35] G. Roati, M. Zaccanti, C. D'Errico, J. Catani, M. Modugno, A. Simoni, M. Inguscio, and G. Modugno, 39K Bose-Einstein Condensate with Tunable Interactions, *Phys. Rev. Lett.* **99**, 010403 (2007).
- [36] N. B. Jørgensen, G. M. Bruun, and J. J. Arlt, Dilute fluid governed by quantum fluctuations, *Phys. Rev. Lett.* **121**, 173403 (2018).
- [37] T. G. Skov, M. G. Skou, N. B. Jørgensen, and J. J. Arlt, Observation of a Lee-Huang-Yang fluid, *Phys. Rev. Lett.* **126**, 230404 (2021).
- [38] C. R. Cabrera, L. Tanzi, J. Sanz, B. Naylor, P. Thomas, P. Cheiney, and L. Tarruell, Quantum liquid droplets in a mixture of Bose-Einstein condensates *Science* **359**,

- 301 (2018).
- [39] P. Cheiney, C. R. Cabrera, J. Sanz, B. Naylor, L. Tanzi, and L. Tarruell, Bright Soliton to quantum droplet transition in a mixture of Bose-Einstein condensates, *Phys. Rev. Lett.* **120**, 135301 (2018).
- [40] G. Semeghini, G. Ferioli, L. Masi, C. Mazzinghi, L. Wolswijk, F. Minardi, M. Modugno, G. Modugno, M. Inguscio, and M. Fattori, Self-bound quantum droplets of atomic mixtures in free space?, *Phys. Rev. Lett.* **120**, 235301 (2018).
- [41] G. Ferioli, G. Semeghini, L. Masi, G. Giusti, G. Modugno, M. Inguscio, A. Gallemí, A. Recati, and M. Fattori, Collisions of self-bound quantum droplets, *Phys. Rev. Lett.* **122**, 090401 (2019).
- [42] C. D’Errico, A. Burchianti, M. Prevedelli, L. Salasnich, F. Ancilotto, M. Modugno, F. Minardi, and C. Fort, Observation of quantum droplets in a heteronuclear bosonic mixture, *Phys. Rev. Res.* **1**, 033155 (2019).
- [43] D. Edler, C. Mishra, F. Wächtler, R. Nath, S. Sinha, and L. Santos, Quantum fluctuations in quasi-one-dimensional dipolar Bose-Einstein condensates, *Phys. Rev. Lett.* **119**, 050403 (2017).
- [44] D. Baillie, R. M. Wilson, and P. B. Blakie, Collective excitations of self-bound droplets of a dipolar quantum fluid, *Phys. Rev. Lett.* **119**, 255302 (2017).
- [45] H. Kadau, M. Schmitt, M. Wenzel, C. Wink, T. Maier, I. Ferrier-Barbut, and T. Pfau, Observing the Rosensweig instability of a quantum ferrofluid, *Nature (London)* **530**, 194 (2016).
- [46] I. Ferrier-Barbut, H. Kadau, M. Schmitt, M. Wenzel, and T. Pfau, Observation of quantum droplets in a strongly dipolar Bose gas, *Phys. Rev. Lett.* **116**, 215301 (2016).
- [47] L. Chomaz, S. Baier, D. Petter, M. J. Mark, F. Wächtler, L. Santos, and F. Ferlaino, Quantum-fluctuation-driven crossover from a dilute Bose-Einstein condensate to a macrodroplet in a dipolar quantum fluid, *Phys. Rev. X* **6**, 041039 (2016).
- [48] L. Tanzi, E. Lucioni, F. Fama, J. Catani, A. Fioretti, C. Gabbanini, R. N. Bisset, L. Santos, and G. Modugno, Observation of a dipolar quantum gas with metastable supersolid properties, *Phys. Rev. Lett.* **122**, 130405 (2019).
- [49] F. Böttcher, J.-N. Schmidt, M. Wenzel, J. Hertkorn, M. Guo, T. Langen, and T. Pfau, Transient supersolid properties in an array of dipolar quantum droplets, *Phys. Rev. X* **9**, 011051 (2019).
- [50] L. Chomaz, D. Petter, P. Ilzhofer, G. Natale, A. Trautmann, C. Politi, G. Durastante, R. M. W. van Bijnen, A. Patscheider, M. Sohmen, M. J. Mark, and F. Ferlaino, Long-lived and transient supersolid behaviors in dipolar quantum gases *Phys. Rev. X* **9**, 021012 (2019).
- [51] Z.-H. Luo, W. Pang, B. Liu, Y. Li, and B. A. Malomed, A new form of liquid matter: quantum droplets, *Front. Phys.* **16**, 32501 (2021).
- [52] M. Guo, F. Böttcher, J. Hertkorn, J.-N. Schmidt, M. Wenzel, H. P. Buchler, T. Langen, and T. Pfau, The low-energy Goldstone mode in a trapped dipolar supersolid, *Nature (London)* **574**, 386 (2019).
- [53] S. Sabari, K. Porsezian and P. Muruganandam, Dynamical stabilization of two-dimensional trapless Bose-Einstein condensates by three-body interaction and quantum fluctuations, *Chaos, Solitons and Fractals* **103**, 237 (2017).
- [54] R. Tamilthiruvalluvar, S. Sabari, K. Porsezian and P. Muruganandam, Vortex formation and vortex lattices in a Bose-Einstein condensate with Lee-Huang-Yang (LHY) correction, *Physica E* **107**, 54 (2019).
- [55] L. Tanzi, S. Rocuzzo, E. Lucioni, F. Fama, A. Fioretti, C. Gabbanini, G. Modugno, A. Recati, and S. Stringari, Supersolid symmetry breaking from compressional oscillations in a dipolar quantum gas, *Nature (London)* **574**, 382 (2019).
- [56] F. Böttcher, J.-N. Schmidt, J. Hertkorn, K. S. H. Ng, S. D. Graham, M. Guo, T. Langen, and T. Pfau, New states of matter with fine-tuned interactions: quantum droplets and dipolar supersolids, *Rep. Prog. Phys.* **84**, 012403 (2021).
- [57] J. Hertkorn, J.-N. Schmidt, F. Böttcher, M. Guo, M. Schmidt, K. S. H. Ng, S. D. Graham, H. P. Buchler, T. Langen, M. Zwierlein, and T. Pfau, Density fluctuations across the superfluid-supersolid phase transition in a dipolar quantum gas, *Phys. Rev. X* **11**, 011037 (2021).
- [58] R. P. Smith, R. L. D. Campbell, N. Tammuz, and Z. Hadzibabic, Effects of interactions on the critical temperature of a trapped Bose gas, *Phys. Rev. Lett.* **106**, 250403 (2011).
- [59] R. Lopes, C. Eigen, N. Navon, D. Clément, R. P. Smith, and Z. Hadzibabic, Quantum depletion of a homogeneous Bose-Einstein condensate, *Phys. Rev. Lett.* **119**, 190404 (2017).
- [60] R. Lopes, C. Eigen, A. Barker, K. G. H. Viebahn, M. Robert-de-Saint-Vincent, N. Navon, Z. Hadzibabic, and R. P. Smith, Quasiparticle energy in a strongly interacting homogeneous Bose-Einstein condensate, *Phys. Rev. Lett.* **118**, 210401 (2017).
- [61] N. Navon, S. Piatecki, K. Günter, B. Rem, T. C. Nguyen, F. Chevy, W. Krauth, and C. Salomon, Dynamics and thermodynamics of the low-temperature strongly interacting Bose gas, *Phys. Rev. Lett.* **107**, 135301 (2011).
- [62] R. J. Wild, P. Makotyn, J. M. Pino, E. A. Cornell, and D. S. Jin, Measurements of Tan’s contact in an atomic Bose-Einstein condensate, *Phys. Rev. Lett.* **108**, 145305 (2012).
- [63] D. A. Butts and D. S. Rokhsar, Predicted signatures of rotating Bose-Einstein condensates, *Nature* **397**, 327 (1999).
- [64] R. J. Donnelly, *Quantized vortices in Helium II* (Cambridge University Press, Cambridge, 1991).
- [65] S. Yi, and H. Pu, Vortex structures in dipolar condensates, *Phys. Rev. A* **73**, 061602(R) (2006).
- [66] I. Tikhonenkov, B. A. Malomed, and A. Vardi, Vortex solitons in dipolar Bose-Einstein condensates *Phys. Rev. A* **78**, 043614 (2008).
- [67] M.A. Baranov, Theoretical progress in many-body physics with ultracold dipolar gases, *Phys. Rep.* **464**, 71 (2008).
- [68] M. Klawunn, R. Nath, P. Pedri, and L. Santos, Transverse instability of straight vortex lines in dipolar Bose-Einstein condensates, *Phys. Rev. Lett.* **100**, 240403 (2008).
- [69] M. Klawunn and L. Santos, Phase transition from straight into twisted vortex lines in dipolar Bose-Einstein condensates, *New J. Phys.* **11**, 055012 (2009).
- [70] R. M. Wilson, S. Ronen, and J. L. Bohn, Stability and excitations of a dipolar Bose-Einstein condensate with

- a vortex, *Phys. Rev. A* **79**, 013621 (2009).
- [71] M. Abad, M. Guilleumas, R. Mayol, M. Pi, and D. M. Jezek, Vortices in Bose-Einstein condensates with dominant dipolar interactions, *Phys. Rev. A* **79**, 063622 (2009).
- [72] M. Abad, M. Guilleumas, R. Mayol, M. Pi, and D. M. Jezek, Dipolar condensates confined in a toroidal trap: Ground state and vortices, *Phys. Rev. A* **81**, 043619 (2010).
- [73] F. Malet, T. Kristensen, S.M. Reimann, and G. M. Kavoulakis, Rotational properties of dipolar Bose-Einstein condensates confined in anisotropic harmonic potentials, *Phys. Rev. A* **83**, 033628 (2011).
- [74] R. K. Kumar, and P. Muruganandam, *J. Phys. B At. Mol. Opt. Phys.* **45**, 215301 (2012).
- [75] R. M. Wilson, C. Ticknor, J. L. Bohn, and E. Timmermans, Roton immiscibility in a two-component dipolar Bose gas, *Phys. Rev. A* **86**, 033606 (2012).
- [76] S. Sabari and R. Kishor Kumar, Effect of an oscillating Gaussian obstacle in a Dipolar Bose-Einstein condensate, *Eur. Phys. J. D* **72**, 48 (2018).
- [77] S. Sabari, R. K. Kumar, L. Tomio, Vortex dynamics and turbulence in dipolar Bose-Einstein condensates, *Phys. Rev. A* **109**, 023313 (2024).
- [78] L. Tomio, A. N. da Silva, S. Sabari, R. K. Kumar, Dynamical Vortex Production and Quantum Turbulence in Perturbed Bose-Einstein Condensates, *Few-Body Systems* **65**, 13 (2024).
- [79] S. Sabari, Vortex formation and hidden vortices in dipolar Bose-Einstein condensates, *Phys. Lett. A* **381**, 3062 (2017).
- [80] Y. Li, J. Liu, W. Pang, and B. A. Malomed, Matter-wave solitons supported by field-induced dipole-dipole repulsion with a spatially modulated strength, *Phys. Rev. A* **88**, 053630 (2013).
- [81] X. Jiang, Z. Fan, Z. Chen, W. Pang, Y. Li, and B. A. Malomed, Two-dimensional solitons in dipolar Bose-Einstein condensates with spin-orbit coupling, *Phys. Rev. A* **93**, 023633 (2016).
- [82] B. Liao, S. Li, C. Huang, Z. Luo, W. Pang, H. Tan, B. A. Malomed, and Y. Li, Anisotropic semi-vortices in dipolar spinor condensates controlled by Zeeman splitting, *Phys. Rev. A* **96**, 043613 (2017).
- [83] S. Sabari, R. Sasireka, R. Radha, A. Uthayakumar, L. Tomio, Vortices in Tunable Dipolar Bose-Einstein condensates with Attractive Interactions, *Phys. Rev. A* **111**, 053320 (2025).
- [84] R. M. W. van Bijnen, A. J. Dow, D. H. J. O'Dell, N. G. Parker, and A. M. Martin, Exact solutions and stability of rotating dipolar Bose-Einstein condensates in the Thomas-Fermi limit, *Phys. Rev. A* **80**, 033617 (2009).
- [85] I. Tikhonenkov, B. A. Malomed, and A. Vardi, Anisotropic solitons in dipolar Bose-Einstein condensates, *Phys. Rev. Lett.* **100**, 090406 (2008).
- [86] Y. Li, Z. Chen, Z. Luo, C. Huang, H. Tan, W. Pang, and B. A. Malomed, Two-dimensional vortex quantum droplets, *Phys. Rev. A* **98**, 063602 (2018).
- [87] Y. V. Kartashov, B. A. Malomed, L. Tarruell, and L. Torner, Three-dimensional droplets of swirling superfluids, *Phys. Rev. A* **98**, 013612 (2018).
- [88] A. Cidrim, F. E. A. dos Santos, E. A. L. Henn, and T. Macrì, Vortices in self-bound dipolar droplets, *Phys. Rev. A* **98**, 023618 (2018).
- [89] L. Klaus, T. Bland, E. Poli, C. Politi, G. Lamporesi, E. Casotti, R. N. Bisset, M. J. Mark, and F. Ferlaino, Observation of vortices and vortex stripes in a dipolar condensate, *Nature Phys.* **18**, 1453 (2022).
- [90] T. Bland, G. Lamporesi, M. J. Mark, and F. Ferlaino, Vortices in dipolar Bose-Einstein condensates, *Comptes Rendus Physique* **24**, 133 (2023).
- [91] A. R. P. Lima and A. Pelster, Quantum fluctuations in dipolar Bose gases, *Phys. Rev. A* **84**, 041604(R) (2011).
- [92] R. N. Bisset, R. M. Wilson, D. Baillie, and P. B. Blakie, Ground-state phase diagram of a dipolar condensate with quantum fluctuations, *Phys. Rev. A* **94**, 033619 (2016).
- [93] F. Wachtler and L. Santos, Quantum filaments in dipolar Bose-Einstein condensates, *Phys. Rev. A* **93**, 061603 (2016).
- [94] A. E. Bennett, C. M. Rienstra, M. Auger, K. V. Lakshmi, and R. G. Griffin, Heteronuclear decoupling in rotating solids, *J. Chem. Phys.* **103**, 6951 (1995).
- [95] R. K. Kumar, L. Tomio, B. A. Malomed, and A. Gammal, Vortex lattices in binary Bose-Einstein condensates with dipole-dipole interactions, *Phys. Rev. A* **96**, 063624 (2017).
- [96] P. Muruganandam and S. K. Adhikari, Numerical and variational solutions of the dipolar Gross-Pitaevskii equation in reduced dimensions, *Laser Physics* **22**, 813 (2012).
- [97] R. K. Kumar, P. Muruganandam, L. Tomio, and A. Gammal, Miscibility in coupled dipolar and non-dipolar Bose-Einstein condensates, *J. Phys. Commun.* **1**, 035012 (2017).
- [98] L. Brito, A. Andriati, L. Tomio, and A. Gammal, Breakup of rotating asymmetric quadratic-quartic trapped condensates, *Phys. Rev. A* **102**, 063330 (2020).
- [99] E. Shamriz, Z. Chen, and B. A. Malomed, Suppression of the quasi-two-dimensional quantum collapse in the attraction field by the Lee-Huang-Yang effect, *Phys. Rev. A* **101**, 063628 (2020).
- [100] M. Schmitt, M. Wenzel, F. Böttcher, I. Ferrier-Barbut and T. Pfau, Self-bound droplets of a dilute magnetic quantum liquid, *Nature (London)* **539**, 259 (2016).
- [101] A. L. Fetter and A. A. Svidzinsky, Vortices in a trapped dilute Bose-Einstein condensate, *J. Phys.: Condens. Matter* **13** R135 (2001).
- [102] R. K. Kumar, T. Sriraman, H. Fabrelli, P. Muruganandam, and A. Gammal, Three-dimensional vortex structures in a rotating dipolar Bose-Einstein condensate, *J. Phys. B: At. Mol. Opt. Phys.* **49**, 155301 (2016).
- [103] G. Baym and C. J. Pethick, Ground-state properties of magnetically trapped Bose-condensed rubidium gas, *Phys. Rev. Lett.* **76**, 5 (1996).
- [104] F. Dalfovo and S. Stringari, Bosons in anisotropic traps: ground state and vortices, *Phys. Rev. A* **53**, 2477 (1996).
- [105] L. Pitaevskii and S. Stringari, *Bose-Einstein Condensation and Superfluidity*, Oxford University Press, Oxford, 2016 (see page 472).